PHYSICAL REVIEW E **90**, 062319 (2014)

Evaluation of x-ray Brillouin scattering data

U. Buchenau*
Jülich Center for Neutron Science, Forschungszentrum Jülich Postfach 1913, D–52425 Jülich, Federal Republic of Germany
(Received 28 February 2014; revised manuscript received 4 August 2014; published 31 December 2014)

Making use of the classical second-moment sum rule, it is possible to convert a series of constant-Q x-ray Brillouin scattering scans (Q momentum transfer) into a series of constant frequency scans over the measured Q range. The method is applied to literature results for the longitudinal phonon dispersion in several glass formers. The constant frequency scans are well fitted in terms of a Q-independent phonon damping depending exclusively on the frequency, in agreement with two recent theories of the boson peak. The method allows us to link the x-ray Brillouin scattering to the diffuse Umklapp scattering from the boson peak vibrations at higher momentum transfer on an absolute intensity scale.

DOI: 10.1103/PhysRevE.90.062319 PACS number(s): 64.70.P−, 78.35.+c, 63.50.Lm

I. INTRODUCTION

Our knowledge of the sound waves at and above the boson peak in glasses is to a large part due to x-ray Brillouin scattering measurements [1–6], which allow us to see the longitudinal part of the sound wave motion in the frequency range between 2 and 20 meV. The experimental arrangement makes scans of $S(Q,\omega)$ at constant momentum transfer Q much easier than constant-ω scans [3]. It is usual to fit such a constant-Q scan in terms of the damped harmonic oscillator function, the so-called DHO

$$\frac{S(Q,\omega)}{S(Q)} = f_Q\delta(\omega) + \frac{1-f_Q}{\pi}\,\frac{\Omega_Q^2\Gamma_Q}{\left(\omega^2-\Omega_Q^2\right)^2+\omega^2\Gamma_Q^2}. \quad (1)$$

Here symbols with the index Q depend on the momentum transfer Q, but *not* on the frequency ω. Ω_Q is the sound wave frequency, which defines the sound velocity $c_Q = \Omega_Q/Q$ at this Q; Γ_Q is the damping of the sound wave, and f_Q is the elastic (in liquids quasielastic) fraction of the scattering at this Q.

The weak point of this evaluation is the following: The strong damping that one fits to the sound waves above the boson peak is not a real physical damping of the vibrations at the sound wave frequency. Instead, it reflects a deviation of the eigenvectors from a perfect sine function in space. Thus, it is not a damping for all frequencies at fixed Q, as supposed by Eq. (1), but rather a distribution of sound wave vectors around an average one at the given frequency. It is a property of the frequency window rather than a property of the momentum transfer window. In fact, this weak point can be directly seen at larger Q, where the DHO fit has too much intensity close to the elastic line [1].

On the other hand, at most points in the relevant (Q,ω)-space, the DHO manages to fit the data very well. Thus, it certainly supplies a good parameter set for the description of $S(Q,\omega)$. The question is only whether the parameters are indeed meaningful. There will be two well-studied cases—silica and glycerol—where they are not, at least not at higher frequencies.

The present paper introduces a method to convert a sequence of DHO fits over a whole range of Q into the set of constant frequency scans that one needs, making use of the classical second moment sum rule [7]. The method is applied to measurements in beryllium fluoride [8], vitreous silica [5], polybutadiene [9], and glycerol [4]. The data are fitted in terms of the phonon structure factor of generalized hydrodynamics [10], which according to two recent theories of the boson peak [11–13] is also appropriate for glasses.

At higher momentum transfer, the scattering is no longer dominated by the longitudinal sound waves but begins to reflect the full vibrational density of states (the Umklapp scattering [14]). This crossover requires the introduction of an additional Umklapp term in polybutadiene and glycerol.

The following Sec. II derives the equation for the dynamic structure factor and its fitting function. Section III applies the equations to the four above-mentioned examples. The fit parameters are compared to the DHO parameters. For beryllium fluoride and polybutadiene, where both parameter sets agree within experimental error, the results are compared to the predictions of one of the theories [13]. Section IV discusses and concludes the paper.

II. THEORETICAL BASIS

Fortunately, it is easy to translate a set of DHO measurements at a series of different Q into the set of constant-ω scans that one would like to have. One notes first that for a DHO $(1-f_Q)S(Q)$ is fixed to the value

$$(1-f_Q)S(Q) = \frac{k_BT}{Mc_Q^2} \quad (2)$$

by the classical second moment sum rule [7],

$$\int_{-\infty}^{\infty}\omega^2 S(Q,\omega)d\omega = \frac{k_BTQ^2}{M}, \quad (3)$$

where M is the average atomic mass. The second moment sum rule has already been successfully used to normalize x-ray Brillouin data in liquid lithium [15], in liquid cesium [16], as well as in glassy sulfur [17] and glassy sorbitol [18].

With this equation, one can calculate a constant-ω scan of $S(Q,\omega)$ for any ω in absolute units, each DHO scan supplying a point at its Q value. The result is best plotted in terms of the

*buchenau-juelich@t-online.de

dimensionless dynamical structure factor $F_\omega(Q)$ defined by

$$F_\omega(Q) = \frac{M\omega^3 S(Q,\omega)}{k_B T Q^2}, \tag{4}$$

which in terms of the DHO parameters is given by

$$F_\omega(Q) = \frac{1}{\pi}\frac{\Gamma_Q \omega^3}{\left(\omega^2 - \Omega_Q^2\right)^2 + \omega^2\Gamma_Q^2}. \tag{5}$$

The definition allows us to link the low-Q x-ray Brillouin scattering results to inelastic x-ray or neutron scattering measurements of the vibrational density of states [19–23] at higher momentum transfer. As one passes the boundary of the first Brillouin zone and approaches the first sharp diffraction peak, one begins to see the whole density of vibrational states in the given frequency window, of which the longitudinal sound waves are only a small fraction. At high momentum transfer, the coherent scattering cross section approaches the incoherent one, in which all vibrations appear on the same intensity level. This high-momentum transfer scattering is called "diffuse Umklapp scattering" [22], because it is the glassy counterpart of the Umklapp scattering from phonons in crystals [14].

The classical one-phonon approximation for incoherent scattering reads

$$S_{\rm inc}(Q,\omega) = \frac{k_B T Q^2 e^{-2W}}{2M}\frac{g(\omega)}{\omega^2}, \tag{6}$$

where $g(\omega)$ is the vibrational density of states and e^{-2W} is the Debye-Waller factor. This shows that within the range of validity of the one-phonon approximation, $F_\omega(Q)$ is related to the oscillation function $S_\omega(Q) = S(Q,\omega)/S_{\rm inc}(Q,\omega)$, which oscillates around 1 at higher momentum transfer,

$$F_\omega(Q) = S_\omega(Q)\frac{\omega g(\omega)}{2}e^{-2W}. \tag{7}$$

$S_\omega(Q)$ contains information on the modes in the given frequency window [23]. Within the classical one-phonon approximation, the oscillation function

$$S_\omega(Q) = \left\langle \frac{3}{Q^2 F_{\rm norm}}\left|\sum_{j=1}^{N} b_j e^{-i\mathbf{Q}\cdot\mathbf{r}_j}\frac{\mathbf{Q}\cdot\mathbf{e}_j}{M_j^{1/2}}\right|^2\right\rangle_\omega, \tag{8}$$

where the angular brackets denote an average over all eigenmodes at the frequency ω, together with a directional average over the momentum transfer vector $\mathbf{Q}$. The sum $j = 1,..N$ goes over the N atoms of the sample, with the position vector $\mathbf{r}_j$, the scattering length b_j and the eigenvector component $\mathbf{e}_j$. The mode normalization factor $F_{\rm norm}$ is given by

$$F_{\rm norm} = \sum_{j=1}^{N}\frac{b_j^2\mathbf{e}_j^2}{M_j}. \tag{9}$$

In a monatomic substance, the translational invariance condition $\sum_{j=1}^{N}\mathbf{e}_j = 0$ ensures an initial Q^2 rise of $S_\omega(Q)$ and thus also of $F_\omega(Q)$. The results of the present work suggest the existence of such an initial Q^2 rise in polyatomic glasses as well.

In order to fit $F_\omega(Q)$ in the Brillouin range, one can use the dynamic structure factor of a damped longitudinal phonon [10–13] plus the initial Umklapp term

$$F_\omega(Q) = \frac{f_\omega}{\pi}\frac{(\Gamma_\omega/\omega)Q^2Q_B^2}{\left(Q^2 - Q_B^2\right)^2 + (\Gamma_\omega/\omega)^2Q^4} + f_U Q^2, \tag{10}$$

with parameters that no longer depend on Q. Instead, they depend on ω as they should. The Brillouin wavevector Q_B defines a frequency-dependent longitudinal sound velocity $c_l = \omega/Q_B$ and Γ_ω describes the frequency-dependent damping. One can no longer reckon with the normalization property of the second moment sum rule. Therefore, one needs not only the two parameters Q_B and Γ_ω, but an additional normalization factor f_ω as well, which tends to one at frequency zero. At higher momentum transfer, one has to include the initial rise $f_U Q^2$ of the Umklapp scattering [19–23].

In generalized hydrodynamics [10], the first term of Eq. (10) is a consequence of the viscous damping, but in the two theories of Schirmacher [11,12] and the very recent one of DeGiuli *et al.* [13], the term results from genuine theoretical treatments of the boson peak. In the original Schirmacher theory [11], the phonon form factor results from fluctuating elastic constants, but it was shown later that one gets the same form factor if one assumes an interaction between soft local oscillators and the sound waves [12]. The second theory (denoted in the following as DLDLW theory) emphasizes the connection between boson peak modes and local structural instabilities, treating the glass as a nearly unstable substance that can be pushed into instability by a small external influence (in the DLDLW theory a small pressure). The dynamic equations are then expanded in terms of the small distance from instability. This leads to a frequency ω^*, the lower boundary of the domain where the phonon damping dominates. The boson peak frequency ω_b and the Ioffe-Regel crossover lie below this ω^* and are pushed down to the frequency zero as one approaches instability. The relation of the parameters of Eq. (10) to the complex modulus $\Delta k(\omega)$ (more precisely the longitudinal modulus multiplied with the mass density, the square of the sound velocity) of the theory is

$$\Delta k(\omega) = \frac{\omega^2}{Q_B^2} + i\frac{\Gamma_\omega\omega}{Q_B^2}, \tag{11}$$

yielding the complex wavevector

$$q^* = \frac{\omega(\mathrm{Re}\sqrt{\Delta k} - i\,\mathrm{Im}\sqrt{\Delta k})}{|\Delta k|}. \tag{12}$$

Note that the real part Q_B^* of this complex eigenvector is *smaller* than Q_B, the more so the stronger the damping is. As an important consequence, the sound velocity ω/Q_B^* is *larger* than ω/Q_B. This consequence holds generally for both theories, but the DLDLW theory [13] emphasizes the difference and makes detailed predictions for the two sound velocities and the mean free path.

III. COMPARISON TO EXPERIMENT

Comparing the DHO with the constant-frequency Eq. (10), one finds complete equivalence for the generic case of a frequency-independent sound velocity together with a damping $\propto Q^2$. Then for $Q = Q_B$ and $\omega = \Omega_Q$, $\Gamma_Q = \Gamma_\omega$. This seems to hold in beryllium fluoride, our first example.

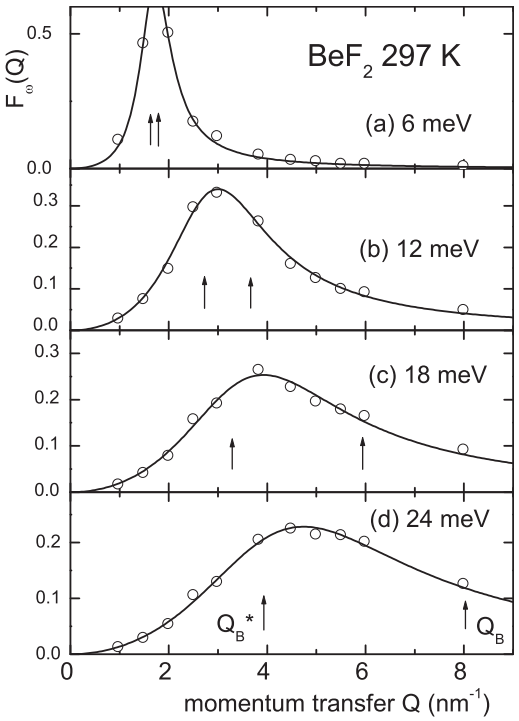

FIG. 1. Constant-ω scans of the dynamic structure factor $F_\omega(Q)$ calculated from the x-ray Brillouin scattering data of Scopigno *et al.* [8] in BeF_2 at 297 K. The lines are fits in terms of Eq. (10) with $f_\omega = 1$ and $f_U = 0$. The arrows denote the two wavevectors Q_B^* and Q_B, of which the smaller one is the true wavevector according to theory [11–13].

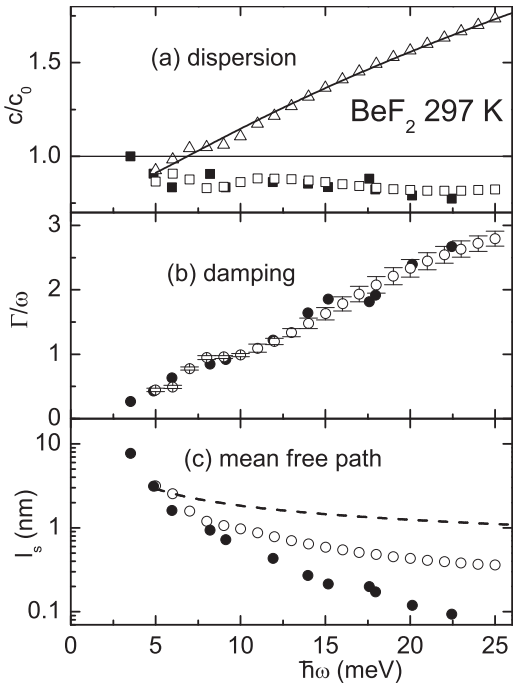

FIG. 2. Comparison of our structure factor fit parameters for beryllium fluoride with the DHO parameters [8] and with the DLDLW theory [13] for (a) the sound velocities (full squares, DHO; open squares, ω/Q_B; open triangles, ω/Q_B^*; continuous line, DLDLW theory with $\omega^* = 5$ meV), (b) the damping (full circles, DHO; open circles, Γ_ω/ω), and (c) the mean free path (open circles, l_s from this work; full circles, $l_{\rm res}$ from the DHO parameters; dashed line, DLDLW theory).

Figure 1 shows that one can fit the $F_\omega(Q)$ calculated from the BeF_2 x-ray Brillouin data of Scopigno *et al.* [8] with $f_\omega = 1$ and $f_U = 0$ up to 25 meV. Fitting f_U, one gets 0 within experimental error. At low frequency, the fit gets better if one allows for f_ω slightly larger than 1, but above 10 meV the fitted f_ω is 1 within experimental error. Since one also obtains a reasonably constant sound velocity over the whole frequency range, the conditions for the equality of both sets of parameters are fulfilled—and one gets indeed the same parameters within experimental error from both approaches (see the comparison to the DHO parameters in Fig. 2).

Note that the influence of the Debye-Waller factor e^{-2W} is negligible in the Brillouin signal, because the mean square displacement at the glass transition is of the order of 10^{-3} nm^2 [24]. In the Brillouin range, the Debye-Waller deviation from 1 is therefore of the order of 1% and remains within the error bars.

According to theory [11–13], the real part of the wave vector is not Q_B, but rather the Q_B^* defined in Eq. (12). Figure 1 shows both values as arrows. One sees that indeed Q_B^* is much closer to the peak in $F_\omega(Q)$ than Q_B, which at 24 meV in Fig. 1(d) is nearly a factor of two larger than the peak position.

The DLDLW theory makes a prediction for the sound velocity $c_l^*(\omega) = \omega/Q_B^*$,

$$c_l^*(\omega) = \frac{|\Delta k|}{\mathrm{Re}\sqrt{\Delta k}} \propto (\omega^2 + \omega^{*2})^{1/4}. \qquad (13)$$

Figure 2(a) shows the sound velocities ω/Q_B^* divided by $c_0 = 5500$ m/s (this value was adapted to the lowest DHO point), as open triangles. They follow the prediction of Eq. (13) with $\omega^* = 5$ meV [the continuous line in Fig. 2(a)]. Above ω^*, $v(\omega)$ separates from ω/Q_B in exactly the way predicted by the DLDLW theory [13].

A second prediction of the DLDLW theory concerns the mean free path of the sound waves

$$l_s = \frac{|\Delta k|}{\omega \mathrm{Im}\sqrt{\Delta k}} \propto \frac{(\omega^2 + \omega^{*2})^{1/4}}{\omega}, \qquad (14)$$

which should separate above ω^* from the DHO mean free path $l_{\rm res} = 2(\Omega_Q/Q)/\Gamma_Q$. The comparison to the calculated results in Fig. 2(c) shows that the separation indeed begins at ω^* as predicted, but that it is only half as large as the prediction [the dashed line in Fig. 2(c)].

Question: Why does one only see longitudinal phonons and nothing else in the very large (Q,ω) range of Fig. 1? The question is answered by our next example, vitreous silica. At low frequency, one finds phonon structure factors that are very similar to those of beryllium fluoride in Fig. 1. At 20 meV, the Umklapp scattering begins to attain the same height as the Brillouin peak. This is shown in Fig. 3, combining x-ray Brillouin data at 1620 K [5] with neutron Umklapp scattering data at a nearby temperature, 1673 K [25]. The figure illustrates the technical problem at high frequencies: the x-ray data end

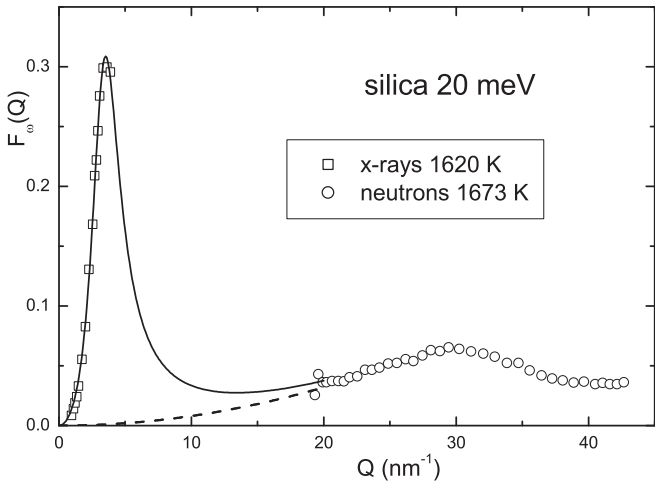

FIG. 3. Constant-ω scan of the dynamic structure factor $F_\omega(Q)$ at 20 meV, calculated from the x-ray Brillouin scattering data of Baldi *et al.* [5] in vitreous silica at 1620 K and from 1673 K neutron data [25]. The continuous line is a fit in terms of Eq. (10); the dashed line is its Umklapp scattering component.

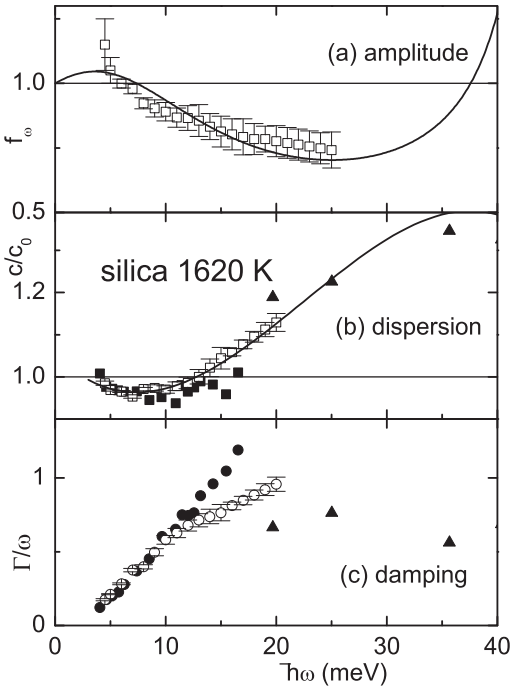

FIG. 4. Structure factor fit parameters for vitreous silica at 1620 K for (a) the amplitude f_ω (open squares), compared to the continuous line calculated from the measured dispersion, (b) sound velocities ω/Q_B normalized to the Brillouin value $c_0 = 6500$ m/s (open squares, this work; continuous line, fit to the open squares; full squares, DHO parameters from the same data [5]; full triangles, DHO parameters from 1570 K data at higher Q [29]), and (c) damping Γ/ω (open circles, this work; full circles, Ref. [5]; full triangles, Ref. [29]).

at 4 nm^{-1} (though they needed not end there); the neutron data begin at 20 nm^{-1}.

Of course, dedicated experiments could close this gap easily and completely. But even with the gap, one understands immediately why the x-ray data [5] can be fitted with $f_U = 0$: The f_U that one extrapolates from the measured Umklapp scattering is too small to influence the fit results (remember that both measurements are on the same absolute intensity scale). Since silica and beryllium fluoride have similar structure and a similar spectrum [21,26], this explains also why one does not see any Umklapp contribution in BeF_2.

The neutron Umklapp scattering shows the peak at 30 nm^{-1} characteristic for librations of corner-connected tetrahedra [23], a motion which does not lead to a large signal at small Q. This might be otherwise (and is indeed otherwise) in other systems: a prominent example are the string-like boson peak modes in glasses forming from simple liquids or in selenium [27], which must be expected to show a large signal already at small momentum transfer. The example illustrates the importance of the method for a better understanding of the interplay between the longitudinal sound waves and the system-specific boson peak vibrations [28].

But though there is as yet no Umklapp scattering in the Brillouin range in silica, f_ω is not 1 as in beryllium fluoride. It shows a gradual decrease in Fig. 4(a) from a value of 1.15 at 4.5 meV to a value of 0.78 at 20 meV. Since the Umklapp scattering cannot be responsible, the deviations of f_ω from 1 at these small Q_B-values must be due to the anomalous dispersion seen in Fig. 4(b). In fact, if one fits the measured sound velocity with a third-order function [the continuous line in Fig. 4(b)], one can calculate f_ω with the equation

$$f_\omega = \frac{c_l}{c_l + \omega \partial c_l / \partial \omega} \tag{15}$$

from the measured sound velocity values $c_l = \omega/Q_B$. This provides the continuous line in Fig. 4(a).

The parameters of fits with $f_U = 0$ between 4.5 and 20 meV in vitreous silica are compared in Figs. 4(b) and 4(c) with the DHO parameters of Baldi *et al.* [5], taking again the Brillouin light scattering sound velocity of 6500 m/s as the reference velocity c_0. One finds differences that are clearly out of the error bars. On the other hand, there is reasonable agreement with DHO values evaluated at higher Q, taking an additional boson peak component into account [29]. This indicates that the differences appear with the appearance of the boson peak in the Umklapp scattering, a phenomenon to which the DHO is naturally more susceptible than a structure factor fit. With the appearance of the boson peak, the apparent DHO sound velocity bends down and the damping increases, unless the boson peak intensity is explicitly taken into account as in Ref. [29].

In the silica case, one sees changes in f_ω from the dispersion without any Umklapp scattering. But there must be a second effect, namely a decrease of f_ω at high frequency, where the weight of the second moment sum rule in $F_\omega(Q)$ is transferred from the longitudinal sound waves to the Umklapp scattering. f_ω must decrease with increasing momentum transfer according to

$$f_\omega = 1 - \frac{Q_B^2}{Q_U^2}, \tag{16}$$

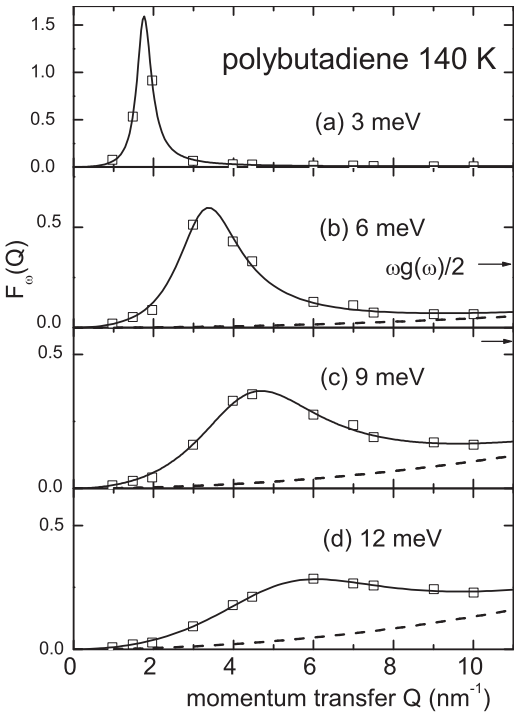

FIG. 5. Constant-ω scans of the dynamic structure factor $F_\omega(Q)$ calculated from the x-ray Brillouin scattering data of Fioretto *et al.* [9] in polybutadiene at 140 K. The continuous lines are fits in terms of Eq. (10); the dashed lines show the Umklapp contribution. The arrows denote the values of $\omega g(\omega)/2$ around which the Umklapp scattering oscillates at high Q.

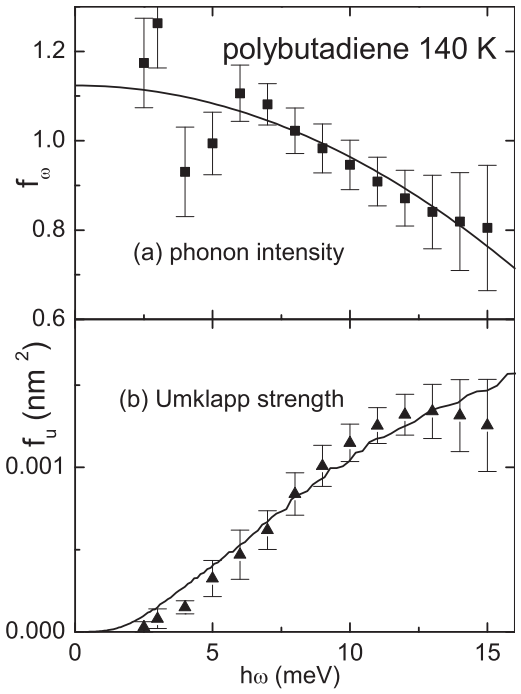

FIG. 6. Evaluation of the 140 K polybutadiene data: (a) Fit (continuous line) of the measured intensity factors f_ω (full squares) in terms of Eq. (16) with $Q_U = 25\,\mathrm{nm}^{-1}$ plus a slight upshift. (b) Comparison of the fitted f_U values (full triangles) with the prediction of Eq. (17) (continuous line) for the same Q_U value, calculated with the measured vibrational density of states [30].

where $\overline{Q_U^2}$ is the weighted average of the Umklapp contributions at the different frequencies with a $Q_U(\omega)$ defined by

$$f_U(\omega) = \frac{\omega g(\omega)}{2Q_U(\omega)^2}. \tag{17}$$

This effect is not seen in beryllium fluoride or in vitreous silica, where the Umklapp scattering is too weak to play a role in the momentum transfer range of the x-ray Brillouin measurements. But it becomes visible in our third example, polybutadiene [9], where the measurements extend up to $10\,\mathrm{nm}^{-1}$ and show a clear Umklapp contribution in Fig. 5. The fits are again perfect up to 15 meV, but do now require a small positive f_U at higher frequencies, as well as a decrease of f_ω from about 1.1 at low frequency to 0.8 at high frequency.

The decrease of f_ω at higher momentum transfer in Fig. 6(a) is well described in terms of Eq. (16) with $Q_U = 25\,\mathrm{nm}^{-1}$ (note there is also a slight influence of the dispersion in Fig. 7(b), which displaces the whole curve to higher values). The same Q_U (together with measured values for the density of states [30]) allows us to reproduce within experimental error the measured f_U values from Eq. (17), as shown in Fig. 6(b). The finding confirms the general considerations on a takeover of the Umklapp scattering at higher momentum transfer which led to the two equations.

The results are again compared to the DHO fits [9] and to the DLDLW theory in Fig. 7, taking the measured [31] light scattering Brillouin sound velocity 2770 m/s as the reference sound velocity c_0. In this case, the fitted value for $\omega^* = 4.2 \pm 0.5$ meV is clearly larger than the boson peak frequency of 2 meV [30], showing that polybutadiene in terms of the DLDLW theory is a glass close to its stability limit. The experimental splitting for the DHO and DLDLW mean free path occurs at ω^* as predicted, but is again weaker than predicted.

Figure 8 shows structure factor scans calculated from x-ray Brillouin data in the last example, glycerol [4]. Their fit reveals a fast disappearance of the longitudinal signal toward higher frequency, together with a fast rise of the Umklapp component. In this case, the disappearing sound wave signal sits on the slope of a broad growing Umklapp scattering mountain, so one does not expect agreement between DHO and constant-frequency parameters. In fact, there is a marked difference in the sound velocity: while the DHO parameters in Fig. 9 show a slight sound velocity decrease at high frequency, the present evaluation shows an increase, similar to the one in silica, but already setting in below the boson peak frequency of 4 meV. Obviously, the silica explanation of the difference is also appropriate here: The DHO gives the wrong answers because the boson peak Umklapp scattering has not been taken into account.

IV. DISCUSSION AND CONCLUSIONS

From the examples in the preceding section, one concludes that the constant-energy scattering form factor, Eq. (10), is indeed able to reproduce the structure factor scans derived

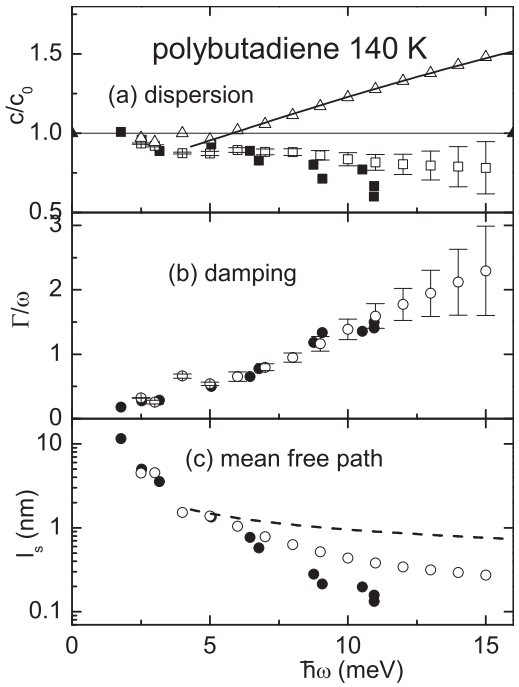

FIG. 7. Comparison of the structure factor fit parameters for polybutadiene determined here with the DHO parameters [9] and with the DLDLW theory [13] for (a) the sound velocities (full squares, DHO; open squares, from ω/Q_B; open triangles, from ω/Q_B^*; continuous line, DLDLW theory with $\omega^* = 4.2$ meV), (b) the damping (open circles, Γ_ω/ω), and (c) the mean free path (open circles, l_s from this work; full circles, $l_{\rm res}$ from the DHO parameters; dashed line, DLDLW theory).

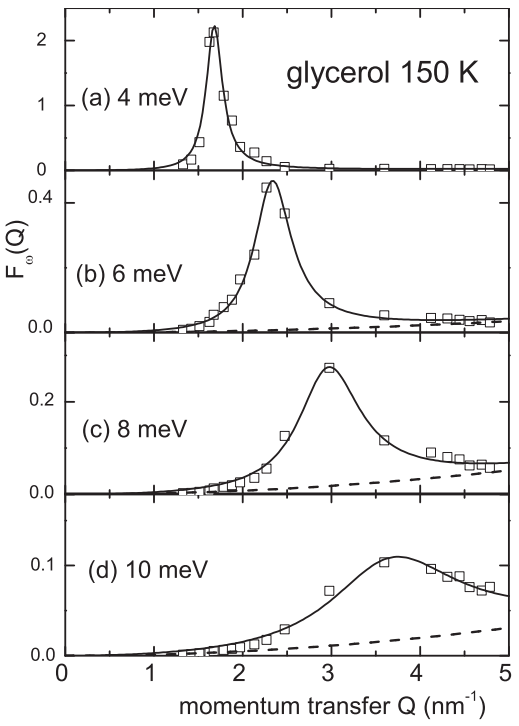

FIG. 8. Constant-ω scans of the dynamic structure factor $F_\omega(Q)$ calculated from the x-ray Brillouin scattering data of Monaco and Giordano [4] in glycerol at 150 K. The continuous lines are fits in terms of Eq. (10); the dashed lines are their Umklapp component.

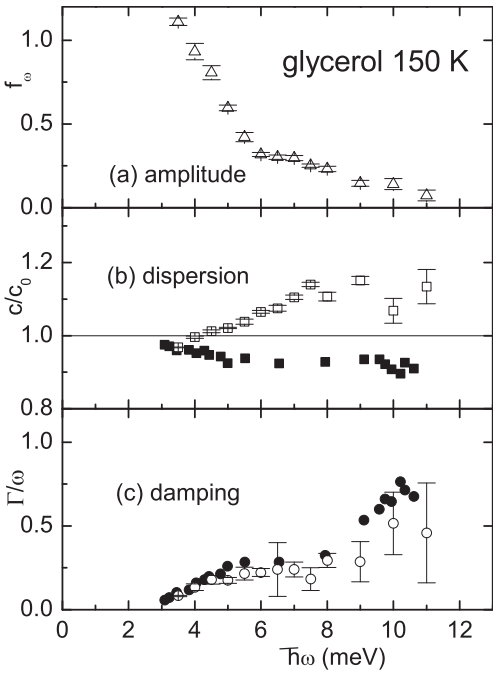

FIG. 9. The parameters of the structure factor fits in glycerol at 150 K for (a) the amplitude f_ω, (b) the sound velocity ω/Q_B divided by the low-frequency sound velocity $c_0 = 3620$ m/s, and (c) the damping Γ_ω/ω. Open symbols from the constant-ω scans of the dynamic structure factor $F_\omega(Q)$; full symbols calculated from the DHO parameters [4].

from DHO data with the second-moment sum rule recipe of the present paper. This confirms the finding of the two theoretical treatments of the boson peak [11–13], according to which the Brillouin scattering form factor of a glass or an undercooled liquid should correspond to the one of generalized hydrodynamics [10].

As emphasized in the DLDLW theory [13], the generalized hydrodynamics form factor implies the existence of two longitudinal sound velocities $c_l^* = \omega/Q_B^*$ and $c_l = \omega/Q_B$, which are equal for zero damping, a natural consequence of a complex modulus. The wave vector Q_B^* determines the oscillation period in space. The examples of beryllium fluoride (Fig. 2) and of polybutadiene (Fig. 4) demonstrate that the DLDLW theory describes the splitting of the two sound velocities at a critical frequency ω^* very accurately. The measured scattering lengths are less well described, probably because the two samples are not close enough to the mechanical instability case, which is the basis of the theory [13]. It is possible to get a better fit to the scattering length with a more refined approximation, which is beyond the scope of this paper.

The sound velocity c_l (the square root of the real part of the complex modulus Δk) is not irrelevant, because it determines the intensity factor. The example of beryllium fluoride (Figs. 1 and 2 of the preceding section) shows that the intensity factor f_ω does not react at all to the large changes in c_l^*, while the example of silica (Figs. 3 and 4 of the preceding section) shows that it is very sensitive to changes in c_l. The wavelength is determined by c_l^*; the intensity of the scattering function is determined by $\partial c_l/\partial\omega$ according to Eq. (15).

The same example illustrates very clearly the origin of possible differences between DHO and structure factor parameters, because they agree if the Umklapp scattering from the boson peak vibrations is properly taken into account [29].

If the measurements extend to higher momentum transfer, one has to add the initial quadratic rise of the Umklapp scattering [19–21,23]. This has been illustrated by the examples of polybutadiene and glycerol. In polybutadiene, this contribution is weak, but in glycerol it tends to dominate the scattering already at the boson peak. The Umklapp parameter brings the number of parameters up to four, one more than those of a DHO fit. When the Umklapp scattering becomes visible, the Brillouin scattering form factor starts to diminish, a second influence on the intensity factor f_ω.

Neither the Schirmacher theory [11] nor the DLDLW theory [13] can predict the Umklapp scattering, because they are continuum theories describing the effect of the atomic disorder in a mean-field approximation. To cite from a new simulation [32] evaluated in terms of the Schirmacher theory, "We would like to emphasize again that the vibrational spectrum beyond the boson peak frequency cannot be described by concepts borrowed from Debyes theory: The disorder is dominant in this regime. It has been shown previously that the vibrational states in this regime obey the statistics of random matrices."

To predict the Umklapp scattering, one needs to calculate the dynamical matrix of the given substance on the atomic level as in the new theoretical approach of Parshin *et al.* [28]. The result depends on the structure factor of substance-specific boson peak modes, thus explaining the very different strength of the Umklapp scattering in our four examples.

Glycerol is not the only glass former showing a disappearance of the longitudinal correlation at relatively low frequency. If one evaluates the selenium Brillouin x-ray data of Scopigno *et al.* [33], one finds the same result. In this case, the longitudinal correlation disappears at 6 meV, the maximum of the dispersion curve derived from the data.

The two examples show an important advantage of the new method. A DHO fit does not tell one how much is left of the full longitudinal correlation, but the fit of the structure factor scans supplies this information.

From the examples shown, it is obvious that one gets more (and more accurate) information from the new evaluation method proposed here, not only because it is better adapted to the physics but also because it allows us to calculate the dynamic structure factor on an absolute scale. For future experiments, it is naturally not necessary to fit with the DHO, because one can apply the second moment sum rule directly to the measured data. This should extend the method beyond the Brillouin scattering into the Umklapp range, where the data are no longer well fitted by the DHO.

To conclude, the classical second moment sum rule allows us to calculate dynamic Brillouin structure factors from damped harmonic oscillator fits of constant-Q scans. The dynamic Brillouin structure factors are not only better adapted to modern theories of the boson peak but are also able to link the Brillouin data to measurements of the full vibrational spectrum at higher momentum transfer on an absolute intensity scale.

ACKNOWLEDGMENTS

Thanks are due to Anne Tanguy for initiating a very helpful workshop on the topic of this paper at Lyon, which led to informative discussions with her, Valentina Giordano, Matthieu Wyart, Eric DeGiuli, Dima Parshin, and Benoit Rufflé.

[1] B. Rufflé, M. Foret, E. Courtens, R. Vacher, and G. Monaco, Phys. Rev. Lett. **90**, 095502 (2003).
[2] B. Rufflé, G. Guimbretiere, E. Courtens, R. Vacher, and G. Monaco, Phys. Rev. Lett. **96**, 045502 (2006).
[3] O. Pilla, A. Cunsolo, A. Fontana, C. Masciovecchio, G. Monaco, M. Montagna, G. Ruocco, T. Scopigno, and F. Sette, Phys. Rev. Lett. **85**, 2136 (2000).
[4] G. Monaco and V. M. Giordano, Proc. Natl. Acad. Sci. USA **106**, 3659 (2009).
[5] G. Baldi, V. M. Giordano, G. Monaco, and B. Ruta, Phys. Rev. Lett. **104**, 195501 (2010).
[6] G. Baldi, M. Zanatta, E. Gilioli, V. Milman, K. Refson, B. Wehinger, B. Winkler, A. Fontana, and G. Monaco, Phys. Rev. Lett. **110**, 185503 (2013).
[7] J.-P. Hansen and I. R. McDonald, *Theory of Simple Liquids*, 2nd ed. (Academic Press, New York, 1986), Ch. 7.4, Eq. (7.4.40), p. 220.
[8] T. Scopigno, S. N. Yannopoulos, D. Th. Kastrissios, G. Monaco, E. Pontecorvo, G. Ruocco, and F. Sette, J. Chem. Phys. **118**, 311 (2003).
[9] D. Fioretto, U. Buchenau, L. Comez, A. Sokolov, C. Masciovecchio, A. Mermet, G. Ruocco, F. Sette, L. Willner, B. Frick, D. Richter, and L. Verdini, Phys. Rev. E **59**, 4470 (1999).
[10] J. P. Boon and S. Yip, *Molecular Hydrodynamics* (McGraw-Hill, New York, 1980), Eqs. (6.3.11) and (6.3.12).
[11] W. Schirmacher, Europhys. Lett. **73**, 892 (2006).
[12] W. Schirmacher, J. Non-Cryst. Solids **357**, 518 (2011).
[13] E. DeGiuli, A. Laversanne-Finot, G. Düring, E. Lerner, and M. Wyart, Soft Matter **10**, 5628 (2014).
[14] G. L. Squires, *Introduction to the Theory of Thermal Neutron Scattering* (Mineola, Dover, New York, 1996).
[15] T. Scopigno, U. Balucani, A. Cunsolo, C. Masciovecchio, G. Ruocco, F. Sette, and R. Verbeni, Europhys. Lett. **50**, 189 (2000).
[16] V. M. Giordano and G. Monaco, J. Chem. Phys. **131**, 014501 (2009).
[17] B. Ruta, G. Monaco, V. M. Giordano, F. Scarponi, D. Fioretto, G. Ruocco, K. S. Andrikopoulos, and S. N. Yannopoulos, J. Phys. Chem. B **115**, 14052 (2011).
[18] B. Ruta, G. Baldi, F. Scarponi, D. Fioretto, V. M. Giordano, and G. Monaco, J. Chem. Phys. **137**, 214502 (2012).
[19] J. M. Carpenter and C. A. Pelizzari, Phys. Rev. B **12**, 2391 (1975).

[20] J.-B. Suck, H. Rudin, H. J. Güntherodt, and H. J. Beck, Phys. Rev. Lett. **50**, 49 (1983).
[21] F. L. Galeener, A. J. Leadbetter, and M. W. Stringfellow, Phys. Rev. B **27**, 1052 (1983).
[22] J. Hafner, Phys. Rev. B **27**, 678 (1983).
[23] E. Fabiani, A. Fontana, and U. Buchenau, J. Chem. Phys. **128**, 244507 (2008), Eq. (11).
[24] U. Buchenau and A. Wischnewski, Phys. Rev. B **70**, 092201 (2004).
[25] A. Wischnewski, U. Buchenau, A. J. Dianoux, W. A. Kamitakahara, and J. L. Zarestky, Phys. Rev. B **57**, 2663 (1998).
[26] R. J. Bell, N. F. Bird, and P. Dean, J. Phys. C **1**, 299 (1968).
[27] H. R. Schober, J. Non-Cryst. Solids **307–310**, 40 (2002).
[28] Y. M. Beltukov, V. I. Kozub, and D. A. Parshin, Phys. Rev. B **87**, 134203 (2013).
[29] G. Baldi, V. M. Giordano, G. Monaco, F. Sette, E. Fabiani, A. Fontana, and G. Ruocco, Phys. Rev. B **77**, 214309 (2008).
[30] U. Buchenau, Prog. Theor. Phys. Suppl. **126**, 151 (1997).
[31] V. N. Novikov, A. P. Sokolov, B. Strube, E. Duval, N. V. Surovtsev, and A. Mermet, J. Chem. Phys. **107**, 1057 (1997).
[32] A. Marruzzo, W. Schirmacher, A. Fratalocchi, and G. Ruocco, Sci. Rep. **3**, 1407 (2013).
[33] T. Scopigno, R. Di Leonardo, G. Ruocco, A. Q. R. Baron, S. Tsutsui, F. Bossard, and S. N. Yannopoulos, Phys. Rev. Lett. **92**, 025503 (2004).